Renewable Energy 270 (2026) 125954

Contents lists available at ScienceDirect

Renewable Energy

journal homepage: www.elsevier.com/locate/renene

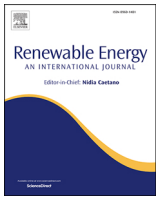

Dual-use wave energy converter arrays: Experimental insights into nearshore processes and coastal erosion

Nadav Cohen [a,*], Francois Flocard [a], Lidong Cui [b], Nataliia Y. Sergiienko [c], Justin S. Leontini [b], Ian L. Turner [a]

[a] Water Research Laboratory, School of Civil and Environmental Engineering, UNSW Sydney, Manly Vale, New South Wales, 2093, Australia
[b] Department of Mechanical and Product Design Engineering, Swinburne University of Technology, Hawthorn, Victoria, 3122, Australia
[c] School of Electrical and Mechanical Engineering, The University of Adelaide, Adelaide, South Australia, 5005, Australia

ARTICLE INFO

Keywords:
WEC array
Oscillating water column (OWC)
Beaches
Sediment transport
Coastal protection
Physical model

ABSTRACT

Wave energy converter arrays have the potential to serve a dual purpose: generating renewable energy while reducing wave energy in their lee and subsequently modifying nearshore processes including wave refraction, diffraction and nearshore currents, all of which influence sediment transport at the shoreline. Understanding the interactions of these physical processes to achieve this dual purpose is complex, and detailed observations to support the design of suitable wave energy converter arrays are lacking. This paper reports on an extensive wave basin experimental program that measured shoreline changes on a sloping, light weight sediment beach, as a function of the incoming irregular wave conditions and five different 16-device wave energy converter array configurations. A key finding is that reducing wave height alone is insufficient for coastal protection; it is also essential to account for wave radiation stresses and the resulting induced currents in the lee of a nearshore wave energy converter array. These currents can lead to zones of shoreline accretion and/or erosion, which are shown to be sensitive to both incident wave conditions and array configuration. Designing wave energy converter arrays for dual use therefore requires careful consideration of nearshore hydrodynamics, sediment transport processes, and site-specific wave conditions.

1. Introduction

Wave energy converters (WECs) inherently reduce incident wave energy by directly extracting energy that is transformed into usable power, and can additionally reduce the wave energy in their lee through the radiated and diffracted wave field. For this reason, arrays of WECs installed near the coast may potentially fulfill a dual purpose of power generation and coastal protection [1]. However, the influence of WEC arrays on nearshore processes and shoreline response remains largely untested in controlled physical experiments.

In coastal engineering, it is well established that conventional coastal protection structures such as emergent or submerged nearshore-detached breakwaters, can alter the wave field through a combination of wave reflection, diffraction, refraction, and/or breaking [2]. The resulting wave energy gradients generate radiation stresses that influence longshore and cross-shore sediment transport, typically leading to localised shoreline accretion and/or erosion [3]. Typical coastal structures such as detached breakwaters are well studied and direct relationships between factors such as breakwater size, distance to shore and the diffracted wave angle are well established [2]. WEC arrays introduce additional complexity. Beyond partial transmission and reflection, they absorb incident energy and radiate phase-shifted waves that interact with neighbouring devices and the surrounding wave field, resulting in the potential for both constructive and destructive interference [4]. The diffracted wave field may range from minimal disturbance to behaviour resembling an impermeable breakwater, depending on array configuration [5]. Consequently, wave height gradients and associated radiation stresses in the nearshore are highly dependent on array layout, device spacing and control strategy, making shoreline response less predictable than for conventional coastal structures.

Numerical and physical modelling approaches have both been used to assess the wave field modifications induced by WEC arrays and their potential coastal impacts. While numerical models provide valuable insights into wave transformation and sediment dynamics, their accuracy relies on validation against real-world deployments and physical experiments, which remain limited in scope, particularly for nearshore

* Corresponding author.
E-mail address: nadav.cohen@unswalumni.com (N. Cohen).

https://doi.org/10.1016/j.renene.2026.125954
Received 22 July 2025; Received in revised form 4 May 2026; Accepted 15 May 2026
Available online 16 May 2026

environments.

Numerical models typically use either phase-averaging or phase-resolving approaches. Phase-averaged models typically represent WECs as partially transmitting and reflecting obstacles, with coefficients for wave transmission and reflection often assumed at various fixed e.g., Refs. [6,7], or wave condition dependent values e.g., Refs. [8,9]. However, these approaches cannot directly account for radiated waves and WEC-to-WEC interactions via multiple-scattering.

Phase-resolving models, (e.g. SWASH), better represent wave scattering, which is crucial for assessing coastal impacts from WEC arrays [10]. The comparison presented in Ref. [11] of an identical WEC array modelled in both SWASH and SWAN broadly showed agreement on the wave height impacts, but notable differences in predicted nearshore currents, highlighting the importance of wave-current interactions for predicting downstream impacts.

Site-specific numerical modelling incorporating sediment transport suggest that shoreline response depends on a range of factors including WEC array distance to shore e.g., Ref. [12], alongshore positioning e.g., Ref. [13] and inter-device spacing e.g., Ref. [14]. These broadly agree with the planar slope bathymetry numerical models in Refs. [9,11], and show that denser arrays and arrays closer to the shoreline tend to result in a narrower but more pronounced area of influence. While many numerical studies indicate reduced beach erosion due to WEC arrays can occur e.g., Refs. [15,16], others e.g., Ref. [17] suggest that under certain wave conditions and array configurations, erosion may increase despite net energy reduction.

Optimisation studies for coastal protection using WEC arrays have explored the effects of PTO damping [18] or array layout [19,20]. However, the objective function in these studies relied entirely on wave height reduction in the lee. Focusing only on wave height neglects other important processes, including nearshore circulation patterns and associated sediment redistribution [19], which have been explored in a limited number of studies e.g., Ref. [21].

Moreover, WEC arrays can be engineered to meet multiple, and sometimes conflicting objectives. These may include: maximising power capture, minimising wave shadowing, and varying device spacing to reduce infrastructure costs [4]. These differing design objectives result in a wide range of configurations, each influencing coastal processes in different ways [19].

The present lack of deployed full-scale WEC arrays along sandy coastlines underscores the importance of physical modelling studies. The specific knowledge gaps addressed in this study include the present lack of physical-model datasets that directly link nearshore WEC arrays, transmitted wave fields, nearshore hydrodynamics and mobile-bed shoreline response. Existing physical studies have largely considered fixed-bed conditions and wave height attenuation only e.g., Refs. [22,23] and typically infer potential shoreline impacts from wave measurements in the lee of the array e.g., Refs. [24,25]. Mobile sediment studies have mainly focused on local scour around individual OWC structures rather than array-scale coastal protection e.g., Refs. [26,27].

This study addresses these gaps through a wave-basin experimental campaign in which five WEC array configurations, each comprising 16 identical bent duct OWC devices, are tested in front of a sloping mobile lightweight-sediment shoreline (Fig. 1). Equivalent baseline cases without any WECs installed were also used for direct comparison. Establishing this linkage is important because the coastal protection function of WEC arrays cannot solely be attributed to wave height attenuation and WEC-induced changes to nearshore currents, sediment transport pathways, and patterns of erosion and accretion in the lee of the array must be considered. The resulting dataset therefore provides both physical insight into shoreline response behind WEC arrays and benchmark data for future numerical model validation. This approach also provides new insights towards the key considerations needed for the dual purpose of energy production with coastal protection, when designing future WEC arrays along sandy coastlines.

Section 2 outlines the experimental setup, followed by Section 3 that presents the results from these experiments, examining the influence of each WEC array configurations on shoreline response and nearshore currents, relative to the Baseline (no WEC) tests. The WEC array configurations are then compared to each other to explore more detailed associations between the wave field and the shoreline and nearshore current responses. The power output of each array is also compared to the shoreline response for all tested array configurations. Section 4 then discusses these results and their limitations in the context of the broader literature, followed by the final Section 5 that presents and synthesises the conclusions of this study.

2. Experimental setup

2.1. Wave basin experimental setup

To ensure broad applicability across scales and sites, the experiments were designed using a generic WEC device and representative nearshore bathymetry, focusing on the relative dimensional proportions of the wave conditions, WEC size and bathymetry, rather than scaling of a specific prototype installation site or WEC design.

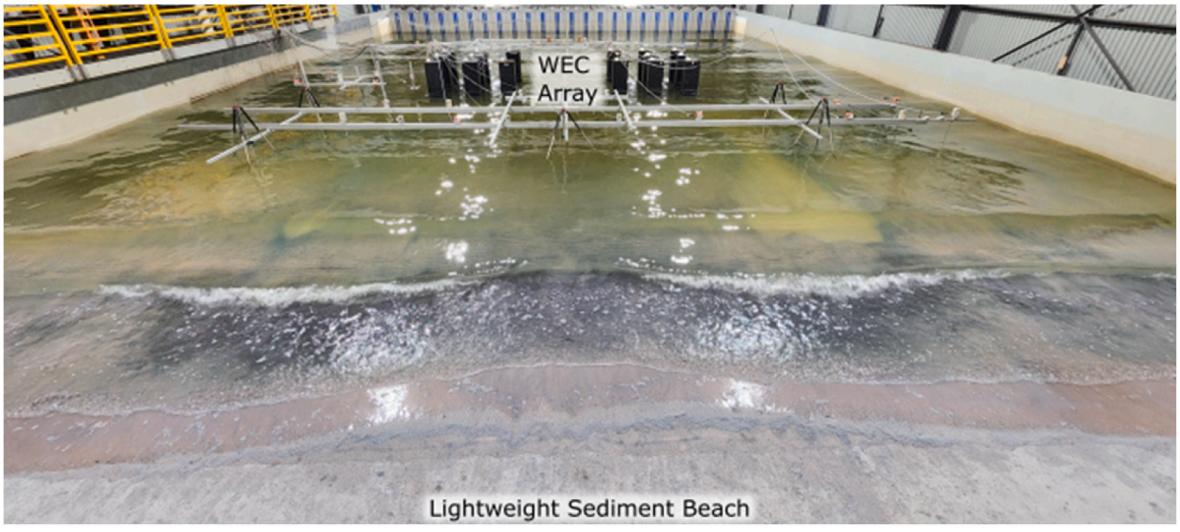

Fig. 1. Overview of the wave basin showing one of the five OWC arrays configurations tested, and the lightweight sediment material used to observe sediment pathways, erosion and accretion at the shoreline.

Testing was conducted at the UNSW Water Research Laboratory, in a 28 m long by 16 m wide wave basin, equipped with a segmented multi-element piston-type wave maker capable of generating multi-directional wave conditions. All tests presented here were conducted with a water depth of 0.586 m measured at the WEC array.

An illustration of the wave basin layout, instrumentation and one of the WEC arrays tested is shown in Fig. 2. A plan view of the basin is shown Fig. 3 and a detailed cross-section overview of the sloped section of the bathymetry is shown in Fig. 4. The basin bathymetry consisted of three sections, extending shoreward from the wave maker to the 'beach'.

1. A 14 m flat section over which the tested OWC's arrays were located,
2. A 7 m long uniform concrete slope of 1V:15H (3.8 deg) extending from the basin floor to 0.116 m below Still Water Level (SWL),
3. A mobile 'beach' section extending from 0.116 m below SWL to 0.098 m above the SWL, reset before each test to the same 1V:15H uniform slope.

Five different 16-device array configurations were positioned in the central region (6.0 m wide by 3.3 m long) of the wave basin. Individual OWCs were rigidly connected to the wave basin floor.

The distance between the front of the shoreward-most OWCs and the landward edge of the beach was kept constant (10.52 m) for all configurations.

Thirty-two capacitance-type wave height probes were distributed around the arrays (Figs. 2 and 3), primarily positioned along three longshore transects, located at distances of 16.90 m (Probe Line 1), 7.80 m (Probe Line 2), and 6.75 m (Probe Line 3) from the landward edge of the beach. The probe spacing was designed to allow wave measurements to be mirrored along the centreline axis of the basin to aid in visualisation of longshore wave height variability. In the following Section 3, the longshore position along the width of the wave basin is referred to as the *x*-axis, with the origin located at the basin centreline.

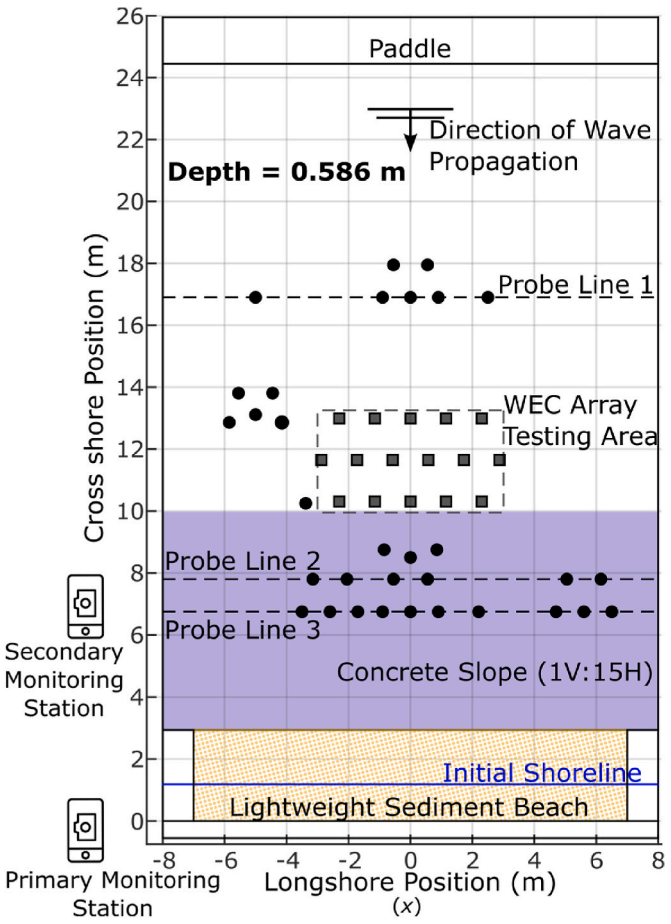

Fig. 3. Plan view of the wave basin showing location of probes (black circles), WEC array area (dashed rectangle) and an example configuration of WECs (black squares). The location of the constant slope bathymetry is shown with the purple area showing the concrete slab and yellow area showing the lightweight sediment beach. Approximate locations of the monitoring stations are also shown. (For interpretation of the references to colour in this figure legend, the reader is referred to the Web version of this article.)

2.2. Lightweight sediment tracer

It is important to note that the inclusion of mobile lightweight sediment in these experiments was not intended to replicate a fully mobile seabed. Instead, the primary purpose was to use this sediment tracer approach that is well-established in the field of coastal engineering studies e.g., Refs. [28,29], to investigate the response and resulting shoreline alignment of an idealised sandy shoreline to the different WEC array configurations tested.

The mobile lightweight sediment material used is composed of granulated polyvinyl chloride (PVC) with a median sediment diameter $D_{50} = 0.39$ mm and density of 1,320 kg/m^3. The use of this lightweight sediment ensured sediment mobilisation for the range of wave conditions used, which would not have been possible using standard density sand (typically quartz) [28]. While lightweight sediment is useful for modelling longshore transport patterns, its use presents scalability challenges due to differences in the relative wet and dry sediment density, limiting accurate representation of scarping behaviour [30].

To ensure consistency, before each test the sediment was redistributed along the beach and reshaped to a constant slope planar beach of 1V:15H. As the sediment naturally redistributed due to the wave action according to slight variations in particle size, care was taken to ensure the sediment was mixed well each time the upper 'beach' section of the profile was reset.

For the purpose of these experiments, these limitations are

Fig. 2. Looking landward in the wave basin showing the three different bathymetry sections. The mobile sediment 'beach' section was reset to the same 1V:15H slope of the adjacent sloping concrete section prior the start of each test. The particular WEC array configuration shown here is "Regular: Three Row" (refer to Section 2.3 and Fig. 7).

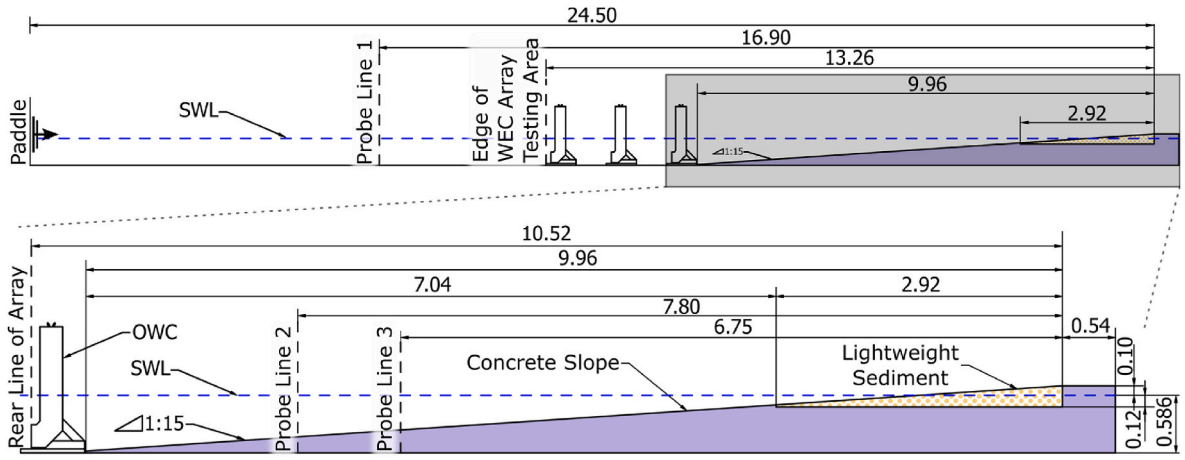

Fig. 4. Cross-section overview of the basin bathymetry (top) and detailed cross section of the sloped section of the bathymetry (below) showing the geometry of the lightweight sediment wedge in yellow, and the still water level (SWL) in blue. (Unit: metres). (For interpretation of the references to colour in this figure legend, the reader is referred to the Web version of this article.)

acceptable and appropriate as, by this approach, no attempt is made to accurately reproduce rates or volumes of sediment transport. Instead, this use of a lightweight sediment tracer material is particularly well-suited to investigating the expected equilibrium planform realignment of a beach (i.e., regions of sediment accumulation and loss, and formation of a salient or tombolo, etc.) in response to a structure constructed in the nearshore [31]. Especially useful to the present study, this methodology was used to identifying sediment transport pathways and the likely processes driving the observed beach planform changes [28].

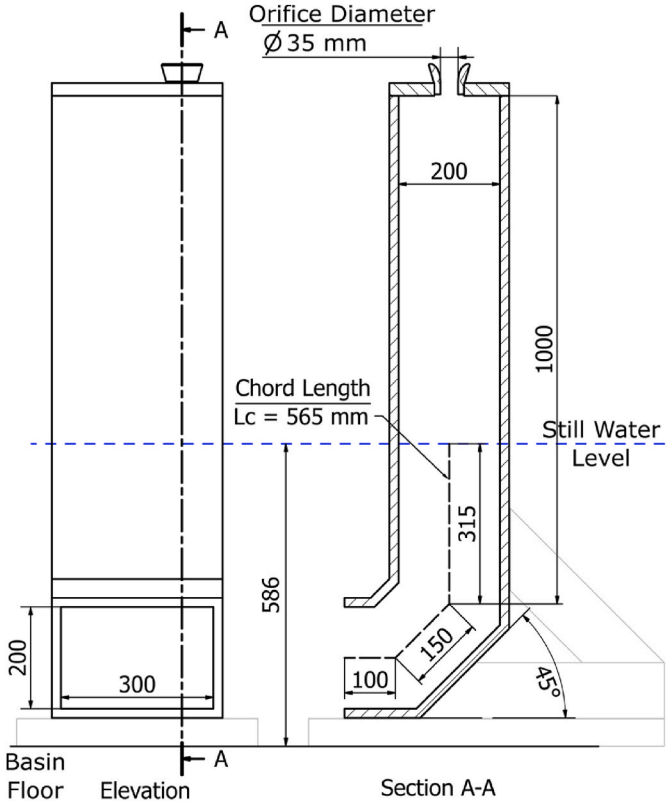

Fig. 5. Dimensioned OWC design (in mm) showing chord length, and position relative to depth of water in basin.

2.3. OWC device and array configurations

The WEC device used for the experiments was the same bent duct OWC geometry previously described and examined in detail in Ref. [32]. Fig. 5 shows the OWC geometry and dimensions. All tests used a constant chord length (L_c = 565 mm) and orifice diameter (Ø = 35 mm). Fig. 6 shows the response amplitude operator (RAO) of the internal water column of the tested OWC, with the peak RAO measured at a period of T = 1.7 s, as reproduced from Ref. [32].

Each of the 16 OWC devices used was fitted with an air pressure sensor measuring the differential pressure between the inside of the OWC to atmospheric. Using the airflow damping coefficient (k) determined in Ref. [33], volume flow (Q_p) was calculated for each tested wave condition using the pressuredata ($p = kQ_p$). The corresponding power output through the orifice for each device was then calculated as $P_{OWC} = pQ_p$. Scaling the air compressibility of OWC air chambers presents an important limitation in the scaling of measured power outputs [34], however as shown in Ref. [32], for the OWCs used in these experiments, air compressibility did not significantly affect wave height transmission in the lee of the OWC. Moreover, the measured power output in these experiments was only used for comparative purpose between arrays.

Five representative WEC array configurations comprising 16 OWC devices were tested, informed by initial array evaluation through physical modelling described in Ref. [33]. These configurations consisted of three 'generic' regularly spaced arrays (arranged in one, two and three rows) and two tailored configurations, as shown in Fig. 7. Comparative assessments were also made against the empty basin (i.e.,

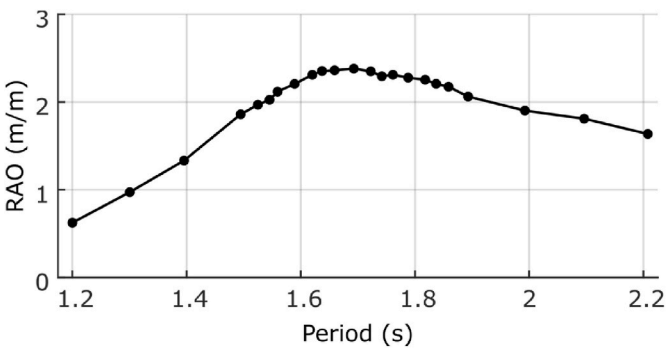

Fig. 6. Response Amplitude Operator (RAO) of the tested OWC, reproduced from Ref. [32]. Markers indicate individual measurements.

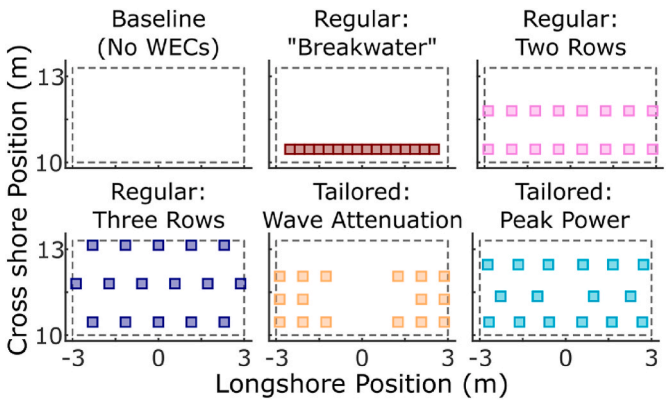

Fig. 7. Plan view of the five WEC array configurations tested, and the 'No WECs' Baseline configuration. Colours are used consistently across all figures to represent the same configuration. (For interpretation of the references to colour in this figure legend, the reader is referred to the Web version of this article.)

no OWC devices), which corresponds to the 'Baseline' configuration shown in Fig. 7.

The two tailored configurations were designed using the numerical optimisation methods described in Ref. [19] using two different optimisation objective goals. The "Tailored: Wave Attenuation" configuration maximised average wave attenuation parallel to the incident wave crests, along a line situated 9.2 m in the lee of the array [35]. The second "Tailored: Peak Power" configuration maximised the OWC internal water column excitation, as a proxy for maximum power output. The optimisation was conducted for monochromatic period $T = 1.5$ s and wave height $H = 0.04$ m. Device spacing was restricted to have a minimum centre-centre spacing of 0.8 m and a symmetric, three row 6-4-6 arrangement aligned with the wave direction axis.

2.4. Wave conditions

The wave conditions used throughout the test program described are summarised in Table 1. A total of 12 individual tests were conducted spanning more than 170 h of wave action.

Testing was undertaken using a repeated sequence of three different irregular wave timeseries, generated using a JONSWAP energy distribution spectrum [36]. This approach is commonly used in both coastal engineering and WEC design studies, to model realistic wave conditions. The JONSWAP spectrum is defined by three parameters: peak enhancement factor (set as 3.3 for this study), significant wave height (H_s), and peak wave period (T_p). Different H_s and T_p defined the three 'Low Energy', 'Medium Energy' and 'High Energy' wave conditions used throughout the testing as specified in Table 1. Each of the wave timeseries extended for ~1000 waves, resulting in duration of ~19 min for the Medium Energy wave condition. As the goal of these experiments was to isolate the effects of the WEC array on the longshore sediment transport, all tests presented in this study were conducted with a shore-normal incident wave field.

Wave basin experiments incorporating mobile sediments typically require long duration tests due to the progressive nature of shoreline realignment processes and the requirement for sufficient time for trends to develop so that robust observations and conclusions can be inferred. For Tests 1-6 (Table 1), each array configuration was tested for a total duration of 17 h of wave action, (~54,000 waves).

To assess the influence of wave conditions, additional tests were conducted without WECs, establishing a Baseline for each test sequence, as well as using the two Tailored Configurations. In these tests, the beach was first conditioned with 18,000 waves of the Medium Energy condition. For Tests 7-9, the wave condition was switched to the Low Energy condition for 24,000 waves, while for Tests 10-12 the wave condition was switched to the High Energy condition for 12,000 waves.

The significant wave height (H_s) at each wave probe was measured for the duration of each test, with the local wave transmission coefficient $\left(K_t = \frac{H_s}{H_{si}}\right)$ at each wave probe calculated using the significant wave height from the corresponding Baseline test as the incident wave height (H_{si}). Wave transmission coefficient curves showing the longshore wave height variation were then produced and compared at the landward-most Probe Line 3 (Fig. 3). As the wave conditions and configurations were symmetrical along the long axis of the wave basin, transmission coefficients for probes were mirrored about the basin centreline to visualise longshore variability of wave heights.

2.5. Shoreline realignment and dye tracer observations

The progression and shoreline realignment of the lightweight sediment beach was monitored using rectified photo derived imagery. Digital images were captured from a fixed position and camera orientation (Fig. 3) between sequences of waves once the water surface within the wave basin quiesced. Images were acquired every 1000 waves for the first 6000 waves, and every 3000 waves thereafter.

The open-source CoastSnap toolbox [37] was used to rectify the image and map the evolving shoreline position. For illustration, Fig. 8 shows an example of the image rectification process and detected shoreline. The use of a changing shoreline position and subsequent beach widths and areas are commonly used in coastal engineering as indicators for beach erosion/accretion as they have been shown to be highly correlated with subaerial beach volume [38].

Shoreline positions were plotted for each timestep to explore the relationship between array configuration, the resulting wave field and the shoreline response. To quantify and compare these results a representative planform area of the beach (A) was calculated as the region bounded by shoreline position and the fixed landward edge of the mo-

Table 1
Summary of the test program detailing the wave conditions and test sequence used for each WEC array configuration.

Test Number	WEC Array Configuration Tested	Test Sequence: Number of Waves, Peak Period (T_p) and Significant Wave Height (H_s)	Time per Test (hrs)	Descriptive Name for Wave Conditions
1	No WECs (Baseline)	54,000 waves, $T_p = 1.6$ s, $H_s = 0.050$ m	17	Medium Energy
2	Regular: Breakwater			
3	Regular: Two Rows			
4	Regular: Three Rows			
5	Tailored: Wave Attenuation			
6	Tailored: Peak Power			
7	No WECs (Baseline)	18,000 waves, $T_p = 1.6$ s, $H_s = 0.050$ m	12.5	Medium Energy
8	Tailored: Wave Attenuation	*then*		*then*
9	Tailored: Peak Power	24,000 waves, $T_p = 1.4$ s, $H_s = 0.045$ m		Low Energy
10	No WECs (Baseline)	18,000 waves, $T_p = 1.6$ s, $H_s = 0.050$ m	10	Medium Energy
11	Tailored: Wave Attenuation	*then*		*then*
12	Tailored: Peak Power	12,000 waves, $T_p = 1.8$ s, $H_s = 0.075$ m		High Energy

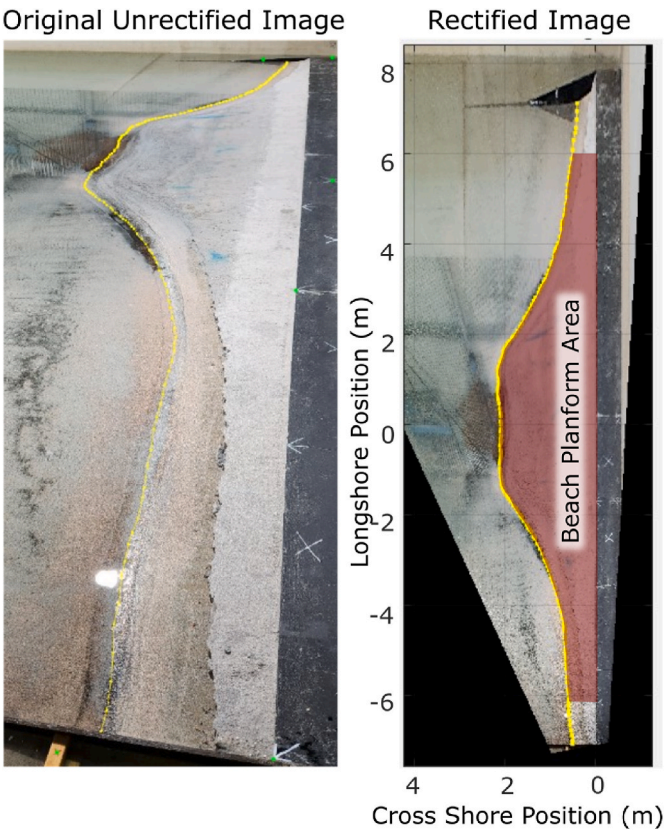

Fig. 8. Example of the image rectification process used to observe and quantify the progression of shoreline realignment of the lightweight sediment 'beach' throughout each test. The plotted shoreline is indicated in yellow and the region used to calculate the beach planform area (which excludes the beach ends) is highlighted in red. (For interpretation of the references to colour in this figure legend, the reader is referred to the Web version of this article.)

bile 'beach' (Fig. 8), extending to 6m either side of the basin centreline to exclude potential edge effects adjacent to the wave basin side walls. This beach planform area was then used to calculate the progression of change in area every 1000 waves ($\frac{dA}{dt}$). These metrics are used in the following section to examine shoreline recession and accretion trends.

To identify zones of shoreline sediment accretion and erosion in the lee of each WEC array configuration relative to the corresponding Baseline test, the relative shoreline position at each timestep was calculated by subtracting the shoreline position of the Baseline test from the shoreline position of the corresponding WEC tests at that same timestep. For the results and analyses presented below, a distinction is made between "relative" erosion/accretion where a comparison is made between two shorelines and "absolute" erosion/accretion where a comparison is made between the measured shoreline as each test progressed, relative to its initial position.

Videos of dye tracer releases were recorded from the secondary monitoring station shown in Fig. 3. These observations provided a useful qualitative indication of the current direction observed in the lee of each of the WEC arrays tested, and provided additional insights to the resulting sediment transport pathways.

3. Results

This section presents the results of the experiments, focusing first on the shoreline response in the absence of any WEC arrays to establish the baseline conditions observed in the wave basin. These results are then compared to the shoreline response in the lee of each WEC array configuration. The nearshore current circulation patterns are presented and interpreted to assist in explaining the differing sediment transport pathways and resulting shoreline changes for each WEC array configuration. Following this, more detailed observations are presented exploring the association between wave height shadowing and sediment deposition and erosion as well as the shoreline and nearshore current response to different wave conditions. Finally, the power output of each configuration is compared to the shoreline response using the change in planform beach area over time as a proxy for coastal erosion protection.

3.1. Baseline Testing

As summarised in Table 1, each wave condition test sequence was initially tested without any WEC array in place, establishing the baseline dataset for comparison with the five array configurations shown in Fig. 7.

For all Baseline tests (Tests 1, 7, 10), a landward shift (i.e., recession) of the shoreline was observed, and importantly, the shoreline always remaining parallel to the incident wave crests. For illustration, the absolute position of the shoreline corresponding to Baseline Test 1 following 18,000 waves is shown in Fig. 9 in black. In all Baseline tests, the resulting shoreline was essentially two-dimensional, with limited longshore variability.

Observing the evolution of the planform beach area (A) over the duration of each test provides additional insights into shoreline recession and accretion trends. The time-evolving planform beach area for Baseline Test 1 is shown in Fig. 10 in black, along with the corresponding Tests 2-6 that are discussed in the next section. The shoreline recession trends for this Baseline Test 1 indicates two distinct stages:

1. Stage 1: an initial rapid and large change in planform beach area that persisted for ~6000 waves; followed by
2. Stage 2: a significantly slower rate of continuing shoreline recession.

The shoreline recession observed during Stage 2 was additionally observed to exhibit a decreasing rate of shoreline change, indicating that the shoreline was progressively converging towards an equilibrium position. These trends were reproduced in an additional shorter test (not listed in Table 1) that was terminated after 24,000 waves (7.5 h),

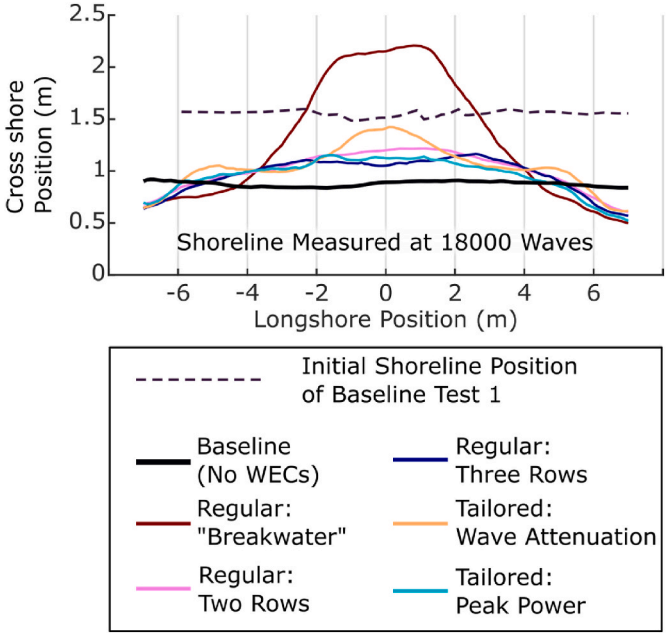

Fig. 9. Absolute shoreline position resulting from Tests 1-8 following 18,000 waves of the Medium Energy wave condition. The initial shoreline position prior to the Test 1 Baseline is shown as a dashed line.

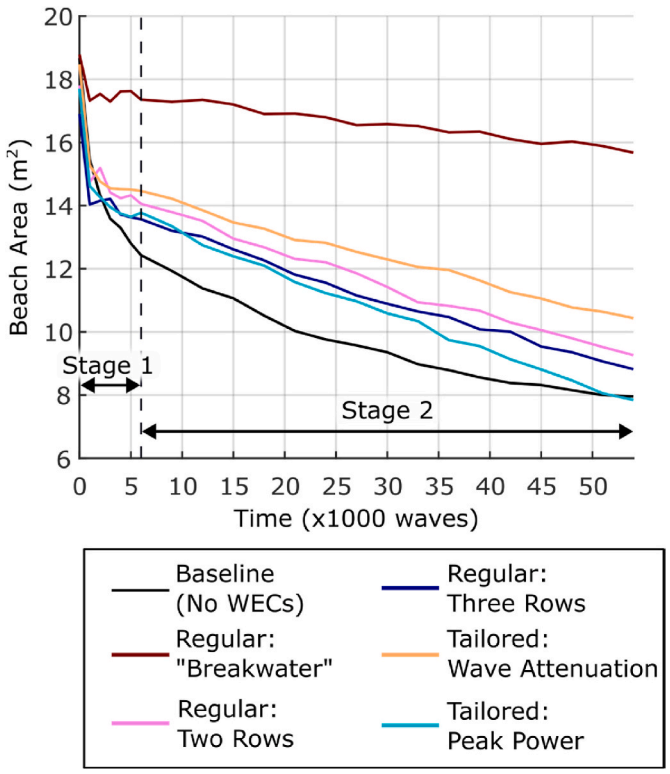

Fig. 10. Planform beach area over time for Tests 1-6 subject to the Medium Energy wave condition. The transition between Stage 1 and 2 shoreline recession trends are indicated with a vertical dashed line.

confirming repeatability of these baseline trends.

For Baseline Test 7 (Table 1), following the initialisation period with the Medium Energy wave condition, the shoreline recession rate under the Low Energy wave condition exhibited highly variable recession for ~6000 waves. This was followed by a similar Stage 2 recession behaviour as Baseline Test 1, albeit at a reduced recession rate.

For Baseline Test 10 (Table 1), under High Energy wave conditions the observed shoreline recession progressed such that after 5000 waves, wave runup began to reach to the non-erodible rigid boundary. Sand replenishment was provided to the exposed rigid boundary, which was quickly eroded prompting termination of this test after 12,000 waves. For this reason, the shoreline recession behaviour could not be confidently determined.

The results from these Baseline Tests 1, 7 & 10 are now used to compare to the various WEC arrays configurations.

3.2. Shorelines and recession trends

Fig. 9 presents the absolute shoreline position after 18,000 waves of the Medium Energy wave conditions for Tests 1-6 (Table 1). Comparison of the shoreline realignment for the WEC array configurations (Tests 2-6) relative to the Baseline (Test 1) consistently show a region of relative sediment accretion along the central portion of the shoreline, and regions of relative erosion near the edges. Only the "Breakwater" Configuration resulted in absolute shoreline accretion, reaching a positional equilibrium between -1.75 m$< x <1.75$ m in Fig. 9. A fully developed equilibrium (i.e., zero net change) in absolute shoreline position was never reached in any WEC array test.

Further insights to shoreline recession and accretion trends for each WEC array test can be inferred from the changing planform beach area (A) over the duration of each test, (Fig. 10). Like the Baseline Test 1, all WEC array Tests 2-6 exhibited two distinct rapid then slower stages in the observed recession trends, with the transition between the two stages occurring at around the same time regardless of array configuration. However, as can be observed in Fig. 10, the Stage 2 shoreline recession behaviour resulted in different characteristic long-term trends with and without the WEC arrays in place. In the presence of a WEC array, during Stage 2, the shorelines were observed to recede at a more constant quasi-linear rate, in contrast to the slowing and converging recession rate of the corresponding Baseline Test 1. By the end of the Medium Energy wave condition, the recession rate ($\frac{dA}{dt}$) of the shoreline in the Baseline test was slower than all other configurations, except for the "Breakwater" Configuration. This is especially well illustrated by the "Peak Power" WEC array configuration (see Fig. 7 for layout). Although the beach area (A) resulting from the "Peak Power" WEC array was larger than that of the Baseline test for most of the test, this difference diminished over time, and the beach area ultimately became smaller due to the difference in the observed rates of recession.

Differences in recession behaviour between the different WEC array configurations and the Baseline test likely reflect WEC-induced changes to nearshore currents and circulation patterns. Dye tracer observations were therefore examined to further investigate the role of nearshore currents in shaping sediment transport patterns and shoreline realignment, as discussed in the following section.

3.3. Nearshore currents and circulation cells

Further insight into nearshore currents and sediment pathways in the lee of the WEC arrays was obtained from dye tracer releases tracked using rectified video. To illustrate, an overlay of video snapshots of Tests 1-4 obtained at time 0 (the moment of dye release), 3 min then 5 min after this, are presented in Fig. 11, with arrows indicating dominant circulation patterns.

In the Baseline Test 1, the two-dimensional uniform mild slope beach produced well-defined cross-shore currents (Fig. 11(a.1)). In contrast, all WEC arrays generated clear nearshore circulation cells. As illustrated in Fig. 11(b.1-d.1), currents converged alongshore towards the basin centreline, flowed offshore, and recirculated towards the basin edge.

It can be inferred that these nearshore circulation patterns were generated by the radiation stresses resulting from the varying wave heights across the basin, and that the currents generated were mobilising sediment from zones with larger waves to zones with smaller waves. To support this, the measured longshore wave height gradients inferred from the calculated transmission coefficients for each test are shown in Fig. 11(b.2-d.2). There is a clear association between the nearshore current circulation patterns and longshore wave height gradients. The longshore current was observed to shift offshore where the longshore wave height gradient was observed to approach 0 (i.e., zones of unchanging transmission coefficient). This association was particularly noticeable when comparing the current circulation patterns between the "Breakwater" Configuration (Fig. 11(b)) and the other regular WEC array configurations (Fig. 11(c and d)). The relatively large wave height gradients measured in the lee of the "Breakwater" Configuration (Fig. 11 (b.2)) resulted in clearly defined flow offshore in the central area of the basin (Fig. 11(b.1)). In contrast, the lower wave height gradients in the "Two Row" Configuration (Fig. 11(c.2)) and again in the "Three Row" Configuration (Fig. 11(d.2)) resulted in a less concentrated current which spread further from the basin centreline at the approximate region where wave height gradients approached 0 (Fig. 11(c.1, d.1)).

Radiation stresses may also arise from oblique wave fronts generated by diffraction around the arrays. Although not explicitly quantified here, experiments in Ref. [33] with identically spaced WEC arrays (Fig. 7) showed that wave height reduction for the "Breakwater" Configuration was primarily diffraction-driven, whereas the other arrays were dominated by radiated wave fields from WEC-to-WEC interactions. As such, the radiation stresses present in these experiments were primarily a result of the longshore wave height gradients generated by the radiated wave field. However, for the "Breakwater" Configuration, where

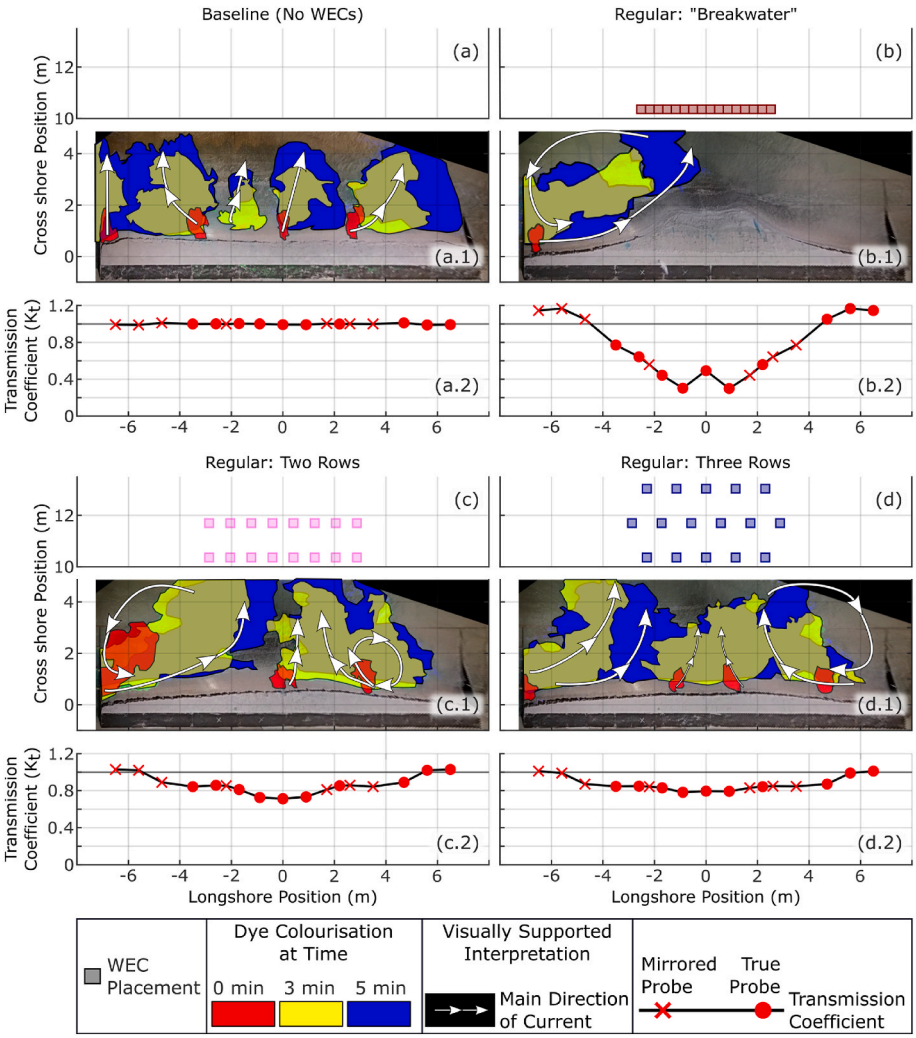

Fig. 11. Overlay of video snapshots at three timestamps for the Baseline (Test 1) and the three regularly spaced WEC array Configurations (Tests 2-4), subject to the Medium Energy wave condition. Extent of dye was colourised for each timestamp (0 min = red, 3 min = yellow, 5 min = blue). White arrows indicated the main direction of the current as supported by visual interpretation the dye movement in the videos. Panels (a – d) indicate the tested WEC configuration. Panels (a.1 – d.1) show the colourised video snapshot overlays. Panels (a.2 – d.2) show the transmission coefficients measured along Probe Line 3. (For interpretation of the references to colour in this figure legend, the reader is referred to the Web version of this article.)

significant wave diffraction occurred, the oblique wave fronts could be expected to induce additional radiation stresses, which could additionally contribute to the more concentrated nearshore current observed and shown in Fig. 11(b.1). As all tests presented in this study were conducted with a shore-normal incident wave field, the observed longshore currents generated by these radiation stresses arose from WEC-induced wave height gradients, not incident wave obliquity.

The contrasting nearshore currents and circulation patterns illustrated in Fig. 11 explain the difference in WEC array versus Baseline shoreline recession trends in Fig. 10. With WEC arrays present, converging longshore currents transported sediment towards the basin centreline and then offshore. In contrast, the absence of a converging longshore current in the Baseline test resulted in a more uniform cross-shore redistribution of the sediment. Consequently, Baseline recession rates decreased as a constant beach slope was approached, whereas WEC array tests continued to recede at a consistent rate. These complex interactions between wave height shadowing and nearshore currents highlight the importance of considering site-specific sediment dynamics and sediment sinks/sources when assessing the long-term coastal impacts of WEC array installations. Factors such as whether sediment demand in sinks is larger than the supply in source areas, and the necessary requirements for sediment depositions should therefore be considered.

3.4. *Threshold for sediment deposition*

To explore the relationship between wave height shadowing in the lee of WEC arrays and observed patterns of sediment accretion and erosion at the shoreline, Fig. 12 compares the longshore wave height variation and shoreline evolution during Tests 2-4 (Table 1), corresponding to the three regularly-spaced WEC array configurations (Fig. 7). These arrays were selected as they produced relatively uncomplicated longshore wave height shadowing patterns, aiding interpretation.

Except for one case, all WEC configurations and Baseline tests produced an overall receding shoreline under all wave conditions. The exception was the “Breakwater” Configuration (Fig. 12(a)), which generated zones of absolute shoreline accretion of ~0.75 m seawards from its initial position (Fig. 12(a.2)). It was also the only configuration that resulted in a zone of unchanging shoreline around $x = \pm 1.75$ m, indicating an equilibrium in sediment deposition and erosion within this zone. Outside of this central zone, the shoreline continued to recede as sediment was transported by the generated currents towards the centre and offshore.

Under the Medium Energy wave condition, the Two and Three Row Configurations (Fig. 12(b and c)) resulted in a spatially similar wave

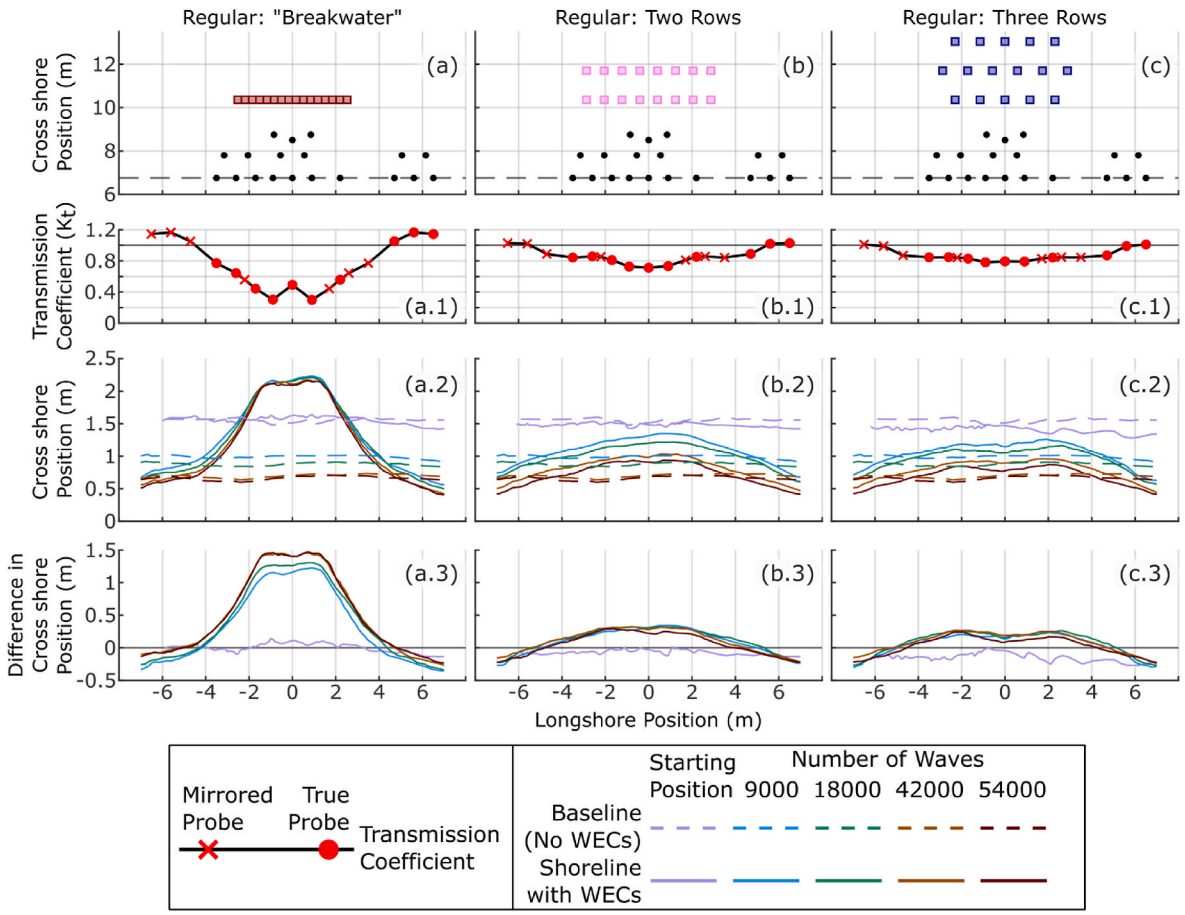

Fig. 12. Results from the regularly spaced WEC array configurations subject to the Medium Energy wave condition (Tests 2-4). Panels (a – d) shows the WEC array configurations with the location of wave probes also indicated (black dot). Panels (a.1 – d.1) shows transmission coefficients measured along Probe Line 3. Panels (a.2 – d.2) shows the absolute shoreline position per timestep in comparison to the No WEC Baseline test. Panels (a.3 – d.3) shows the same shoreline positions relative to the Baseline test (No WECs) shoreline.

height reduction at the measured probe line. The key difference being the magnitude of wave height reduction around the centreline (-1.7 m$\leq x \leq$1.7 m) in the lee of these two configurations (Fig. 12(b.1, c.1)). The transmission coefficient at the central probe was ~10% greater for the Three Row Configuration, with $K_t = 0.71$ and $K_t = 0.79$ for the Two and Three Row Configurations, respectively. Accordingly, the Three Row Configuration resulted in greater shoreline erosion around in central region. This can be seen when comparing Fig. 12(b.3, c.3). However, beyond ±2.2 m from the basin centreline, both configurations exhibited similar shoreline evolution trends.

These observations suggests that a wave height reduction threshold may be necessary for shoreline accretion to occur. If this threshold is not exceeded, sediment mobilisation and offshore transport are likely due to nearshore currents generated by the WEC array. This observation is supported by the large salient formed seen the lee of the "Breakwater" Configuration (Fig. 12(a.2)), and the current circulation patterns observed from dye releases identified in Fig. 11.

3.5. Complex interactions between wave height reduction and shoreline response

The two 'tailored' WEC array configurations (Fig. 7) were obtained by a numerical optimisation method to separately maximise wave height attenuation (Test 5) and peak power output (Test 6). Referring to Fig. 13, both these configurations were observed to result in complex patterns of longshore wave height shadowing.

When tested with the Medium Energy wave condition, the "Wave Attenuation" Configuration (Test 5) resulted in a distinctive pattern of wave height shadowing at Probe Line 3, with three zones of wave height reduction, occurring at $x = 0$ m and $x = \pm 3.5$ m (Fig. 13(a.1)). This was interspersed with zones of little change in wave height (i.e., $K_t \approx 1$) occurring at $x = \pm 2.2$ m and $x = \pm 5.5$ m. Notably, despite these zones of relatively larger wave heights, the resulting shoreline displayed stable sections between $x = \pm 2.7$ m and $x = \pm 4.8$ m (Fig. 13(a.3)). This distinct shoreline signature is explained by the observation of the converging currents generated in the presence of this particular WEC array configuration, which resulted in sediment being replenished in these zones where the larger waves heights could suggest that erosion was expected.

In contrast, the "Peak Power" WEC array configuration (Fig. 13(b)) produced a relatively uniform shoreline response, similar to the Two and Three Row regularly-spaced WEC array Configurations previously described in Fig. 12. This likely reflects the smaller variation between the local wave height maxima and minima, which were insufficiently distinct to result in a noticeable shoreline response.

The distinctive shoreline response in the "Wave Attenuation" Configuration test – with the shoreline accretion in the lee of an area devoid of WECs – clearly demonstrates that the use of transmission coefficient curves alone is not sufficient to predict shoreline response highlighting a limitation of optimisation approaches based solely on transmission coefficient curves. Additionally, while the symmetrical basin and array layout in these experiments produced converging circulation cells along the centreline, other configurations and/or wave conditions and direction may generate more complex circulation patterns with multiple cells, potentially leading to unintended and

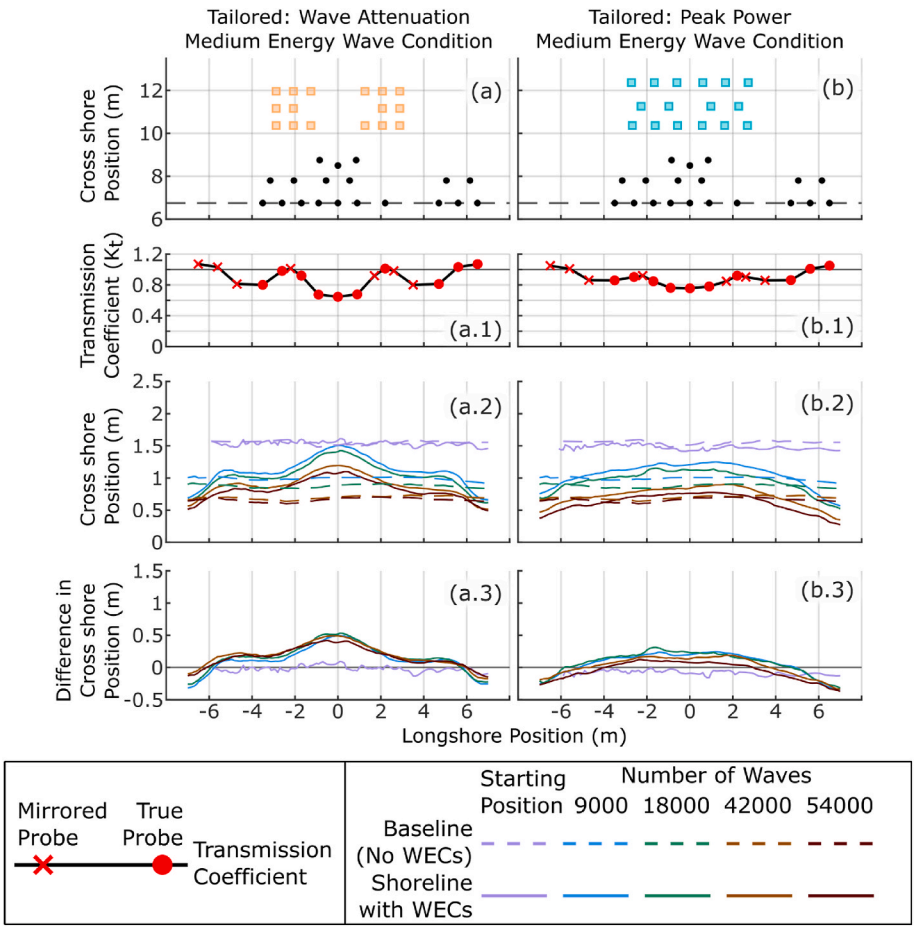

Fig. 13. Results from the tailored WEC array configurations subject to the Medium Energy wave condition (Tests 5 & 6). Panels (a & b) shows the WEC array configurations with the location of wave probes also indicated (black dot). Panels (a.1 & b.1) shows transmission coefficients measured along Probe Line 3. Panels (a.2 & b.2) shows the absolute shoreline position per timestep in comparison to the No WEC Baseline test. Panels (a.3 & b.3) shows the same shoreline positions relative to the Baseline test (No WECs) shoreline.

potentially destructive shoreline impacts regardless of the wave shadowing they produce.

3.6. Nearshore current and shoreline response to varying wave conditions

To investigate how varying wave conditions influence nearshore currents, circulation patterns and the resulting sediment transport at the shoreline within the lee of nearshore WEC arrays, additional tests were conducted under Low Energy (Tests 7-9) and High Energy (Tests 10-12) wave conditions using the test procedure summarised in Table 1.

Fig. 14 presents the relatively subtle variations in the wave height transmission coefficient (K_t) in the lee of the two WEC array configurations across the three wave conditions and the corresponding shoreline positions after 27,000 waves, relative to the Baseline tests. Fig. 15 presents a video snapshot overlays of dye tracer movement for each wave condition, illustrating the inferred nearshore circulation currents.

For both WEC array configurations, an increase in the wave energy resulted in a subtle decrease in variability in transmission coefficient along the measure probe line. For the "Wave Attenuation" Configuration, an increase in wave energy (longer wave period and increased wave height) reduced the K_t maxima at $x = \pm 2$ m, while the minima shifted to $x = \pm 3.6$ m and $x = \pm 5.0$ m for the Low and High Energy wave conditions respectively (Fig. 14(a.1)).

Previous experiments described in Ref. [33] demonstrated that the relative contributions of diffracted and radiated wave fields depend on both WEC array configuration and wave period. In the new experiments presented here, the individual OWC devices were tuned to a peak resonant period of $T = 1.7$ s, which is midway between the peak wave periods of the Medium Energy ($T_p = 1.6$ s) and High Energy ($T_p = 1.8$ s) wave conditions. This is notable, as wave height reduction from the radiated wave field is expected to be greatest at wave periods near the WEC resonance. Accordingly, both array configuration and WEC tuning influence wave height reduction and resulting nearshore radiation stresses.

Significant differences in the observed dye movement in the "Wave Attenuation" Configuration test (Fig. 15(a.1-3)) suggest that the shape of circulation cells were sensitive to the wave energy condition and resulting patterns of wave height reduction. However, common to these three wave energy conditions, the longshore current was observed to shift seawards at the approximate location of K_t increase from the described minima to the maxima leading to a more dispersed and spread out current at $x = \pm 3$ m.

This reduction in K_t variability when the incident wave energy was increased can also be seen to impact the shoreline. When subject to Medium Energy wave conditions the distinct salient shape extending from $x \approx \pm 2$ m about the centreline restricted to a range of $x \approx \pm 1.7$ m for the Low Energy Wave condition, but broadened to $x \approx \pm 3$ m for the High Energy wave condition (Fig. 14(a.2, a.3)).

A similar reduction in K_t variability with increased wave energy was observed for the "Peak Power" WEC array (Fig. 14(b.1)) where K_t range between the outermost and central probe decreased from $0.75 < K_t < 1.1$ under Low Energy wave conditions to $0.81 < K_t < 0.97$ under High Energy wave conditions.

Under High Energy wave conditions, the general increase in wave

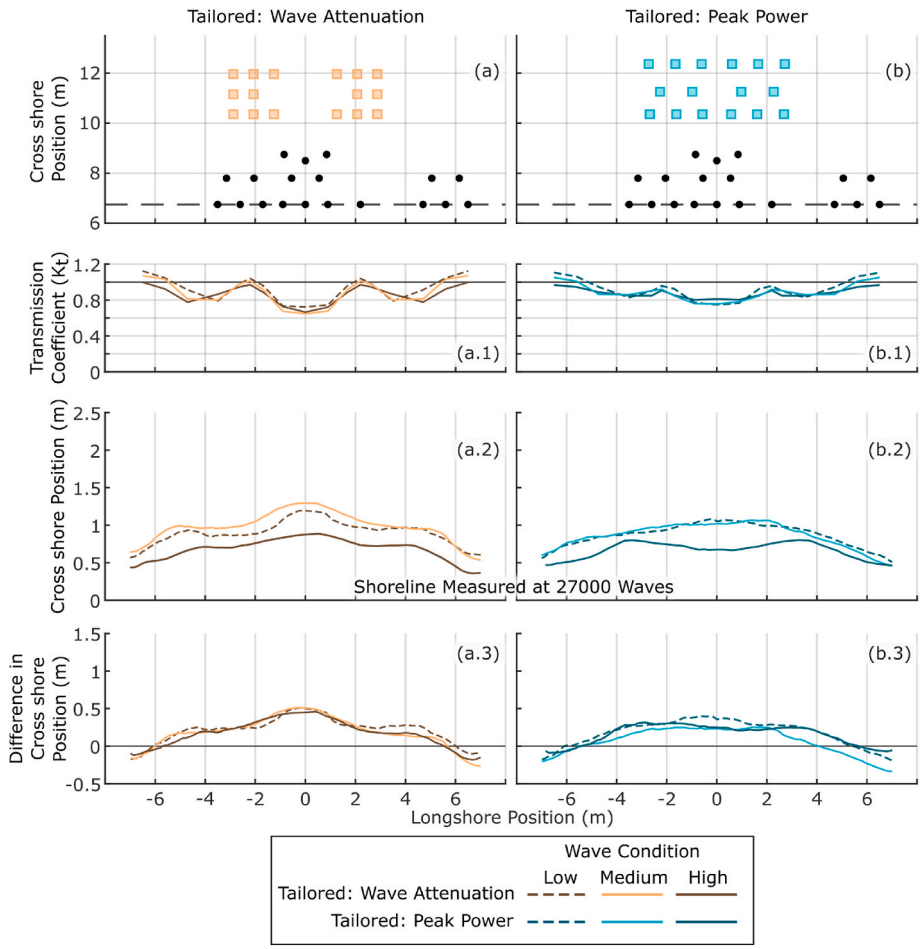

Fig. 14. Results from the tailored WEC array configurations subject to the Low (Tests 8 & 9), Medium (Tests 5 & 6) and High Energy (Tests 11 & 12) wave conditions. Panels (a & b) shows the WEC array configuration with the location of wave probes also indicated (black dot). Panels (a.1 & b.1) shows the transmission coefficients measured along Probe Line 3. Panels (a.2 & b.2) shows the absolute shoreline position per configuration after 27,000 waves. Panels (a.3 & b.3) shows the same shoreline positions relative to the Baseline test (No WECs) shoreline at the respective wave condition.

height transmission resulted in a central zone of relative shoreline erosion as wave heights exceeded the assumed threshold for sediment deposition (Fig. 14(b.2, b.3)). Additionally, Fig. 14(b.1) suggests that the alongshore gradients in wave heights around this central region were low. From Fig. 15(b.3), this can be inferred to have caused the nearshore circulation cell to disperse offshore further away from centre, as the low wave height gradient resulted in a more spread out circulation cell and generated a diverging circulation cell in the central zone.

A smaller central diverging circulation cell was also observed with the "Wave Attenuation" Configuration under High Energy wave conditions (Fig. 15(a.3)). However this circulation cell was observed to have a small alongshore extent and this region was associated with reduced incident wave energy, which may explain why limited shoreline erosion was measured within the central section of the beach.

Varying the wave conditions also influenced the nearshore current velocities inferred from the movement of dye in the wave basin. Contrasting Fig. 15 (a.1, b.1) to (a.3, b.3), the Low Energy wave condition was observed to result in a generally more 'spread out' and reduced velocity nearshore circulation cell whilst the High Energy wave condition was generally observed to result in increased rates of dye dispersion and stronger nearshore currents.

These results demonstrate that nearshore circulation patterns, longshore sediment transport, and shoreline response in the lee of WEC arrays are highly sensitive to the incident wave conditions. Changes in wave energy not only influenced wave transmission but also altered the pattern and velocity of circulation cells and the resulting patterns of sediment erosion and deposition. Importantly, configurations that provided beneficial shoreline outcomes under one wave condition may not necessarily be beneficial under others. This highlights the need to account for the range of expected wave climates when designing WEC arrays for coastal protection.

3.7. Relationship between power output and shoreline response

To complement the primary focus of these experiments on nearshore processes, the total power output was calculated for all array configurations and wave energy conditions listed in Table 1. Fig. 16 compares this power output to the observed changes in planform beach area over time ($\frac{dA}{dt}$) at three distinct stages of testing.

To compare the power output across wave conditions, the total WEC array power output for each configuration was normalised using the average incident wave power per unit crest width for irregular waves (P_w) [39]:

$$P_w = \rho g \int S(\omega) C_g(\omega) d\omega \quad (1)$$

Where $S(\omega)$ and $C_g(\omega)$ describe the frequency dependant energy spectrum and group velocity at the tested depth respectively, and ρ and g are the water density and gravitational acceleration respectively.

The crest width was taken to be the fixed 6 m width of the WEC Array Testing Area (Fig. 3) and therefore the normalised power output was estimated as:

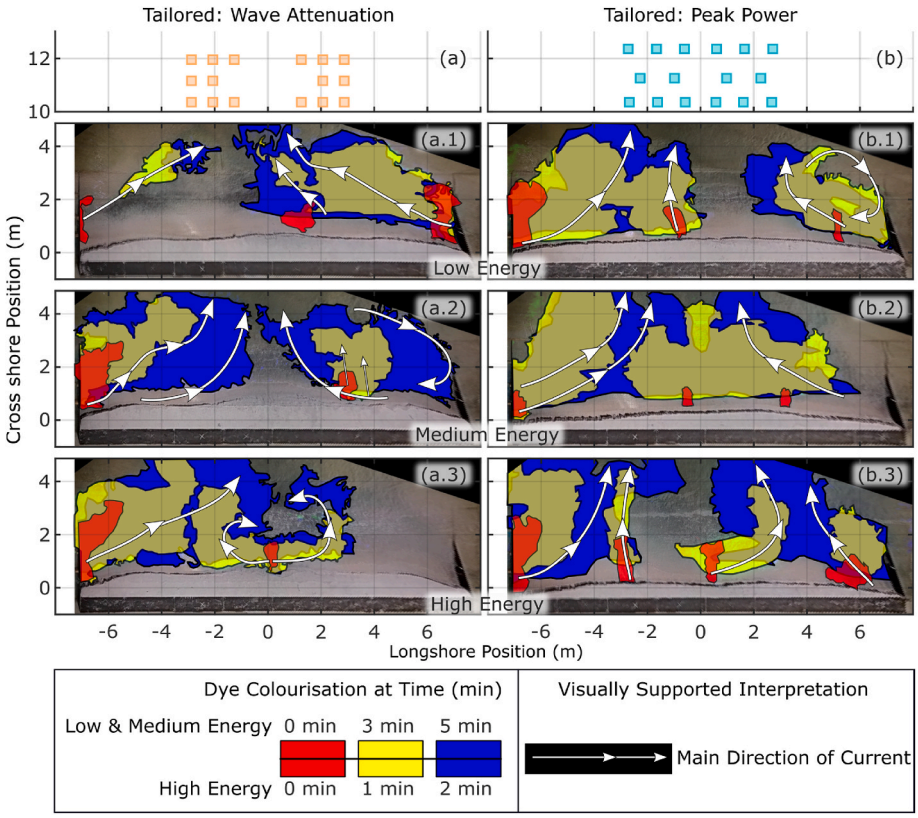

Fig. 15. Overlay of video snapshots at three timestamps for the tailored WEC array configurations (shown in Panels (a & b)), subject to Low (Tests 8 & 9, Panels (a.1 & b.1)), Medium (Tests 5 & 6, Panels (a.2 & b.2)) and High Energy (Tests 11 & 12, Panels (a.3 & b.3)) wave conditions. Extent of dye was colourised for each timestamp. White arrows indicated the main direction of the current as supported by visual interpretation the dye movement in the videos. Note that the High Energy wave condition in Panels (a.3 & b.3) spans 2 min in contrast to the remaining panels spanning 5 min.

$$P_{\text{norm}} = \frac{\Sigma P_{\text{OWC}}}{6 \cdot P_{\text{w}}} \tag{2}$$

Notably, P_{norm} indicates the usable power output measured through the OWC orifice, rather than the power removed from the wave field as it does not account for parasitic power losses through turbulence and drag in and around the OWC.

While the limited number of tests prevents confirmation of quantitative trends, the "Breakwater" Configuration (Fig. 7) was a clear outlier, producing the greatest power output and least beach recession, indicating potential for mixed use of detached breakwaters with OWC devices. For Low and Medium Energy wave conditions, the remaining configurations – where individual OWC devices were spaced apart – showed similar power outputs but a wide range of Stage 2 recession rates ($\frac{dA}{dt}$) varying between -0.124 m^2/1000 waves and -0.084 m^2/1000 waves (Fig. 16(c)).

It is also noted that the numerically optimised "Peak Power" Configuration resulted in a similar power output to that of the "Wave Attenuation" Configuration for all wave conditions, likely because the optimisation was conducted for the monochromatic period $T = 1.5$ s, rather than the irregular wave spectrum used in these experiments.

Additionally, while the tested WEC arrays generally resulted in decreased recession rates relative to the baseline across the full duration of all tests, an increase in the erosion rate was observed in the presence of WECs, relative to the Baseline without WECs during the Stage 1 High Energy wave condition (Fig. 16(b)).

In summary, no clear trend between array power output and beach recession rate could be determined. This is consistent with the results and discussion presented in Section 4.6, which showed substantial differences in wave height transmission, nearshore currents and shoreline response, despite similar power output. This finding is similar to those in Ref. [20] which indicate a widely varying power output for different wave attenuation values. Therefore, a nuanced approach is required when designing and optimising WEC arrays for coastal protection and power output, that must necessarily consider WEC-wave interactions, nearshore hydrodynamics and sediment transport e.g. Ref. [21]. Additionally, future WEC arrays studies incorporating dual-use coastal protection should consider the coastal impacts across the full range of expected wave conditions at any specific site, including both modal and storm conditions.

4. Discussion

From the experiments presented in this paper, a clear shoreline and nearshore response to the tested WEC arrays were observed with the underlying processes identifiable through the analysis presented.

The interactions between the incident wave field and WEC arrays were observed to result in the transmitted wave field propagating to shore. This was influenced by the wave energy absorbed by the WECs; the radiated wave field from the WEC response to the incident wave field and WEC-to-WEC interactions; and the diffracted wave field resulting from interactions between incident wave field and WEC array structure. The transmitted wave field was also visually observed to refract as waves approached shallower depths and interacted with the bathymetry. This transformation is another key consideration for WEC array design, though it was not explicitly explored in these experiments.

The transmitted wave field was in turn observed to influence nearshore current generation and resulting sediment transport at the shoreline, through four primary drivers: wave height, wave height gradients (both longshore and cross-shore), wave period, and wave direction. These drivers interacted with each other and the bathymetry.

All tests presented in this study were conducted with a shore-normal

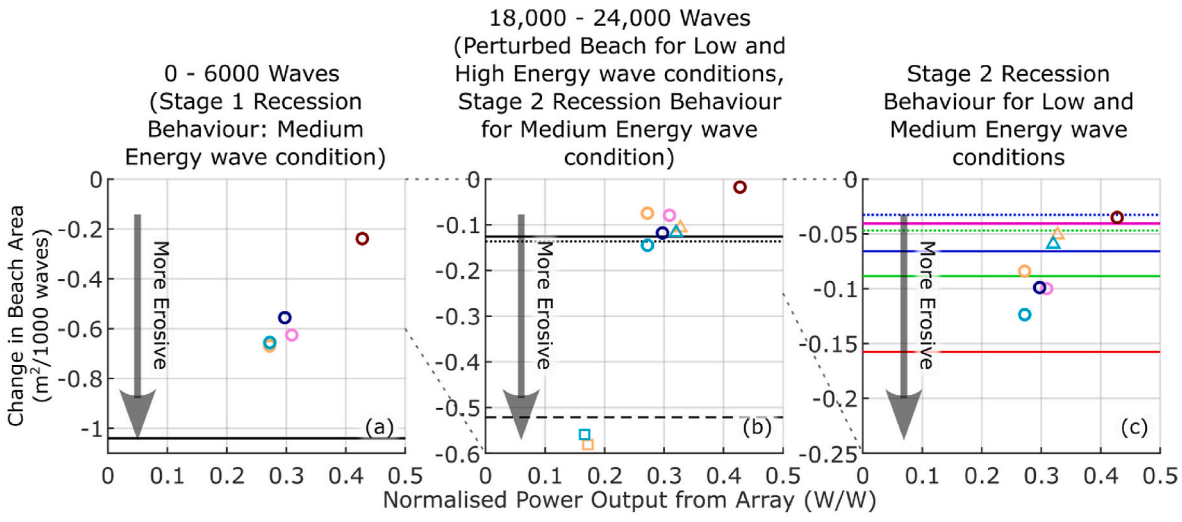

Wave Condition	Breakwater	Two Row	Three Row	Wave Attenuation	Peak Power	Baseline Configuration (No WECs)				
						Panel (a) & (b)	Panel (c)			
						Change in Beach Area between indicated timesteps	3-point average between 27,000 to 42,000 waves		3-point average over entire 54,000 wave test	
							Maximum	Minimum	Maximum	Minimum
Medium Energy	○	○	○	○	○	———	———	———	———	———
Low Energy				△	△	·····	·····	·····	Not Tested	
High Energy				□	□	– – – –	Stage 2 Not Reached		Not Tested	

Fig. 16. Change in planform beach area vs normalised power output from array per 1000 waves ($\frac{dA}{dt}$) at three experimental stages. Panel (a) shows the initial perturbation of the beach (i.e., Stage 1 from 0 to 6000 waves) for the Medium Energy wave condition. Panel (b) shows the perturbation of the b each for a changing wave condition to Low or High Energy wave conditions (18,000 – 24,000 waves), with comparison to the Stage 2 unchanged Medium Energy wave condition. Panel (c) shows the Stage 2, three-point average recession for the Low and Medium Energy wave condition. As steady state for the High Energy wave condition could not be established, it is excluded from Panel (c).

incident wave field, and therefore longshore wave height gradients were not observed for the Baseline tests in which no WECs were present in the wave basin. For these tests, the movement of sediment in the vicinity of the shoreline was predominantly in the cross-shore direction only. However, when WEC arrays were installed in the wave basin, significant longshore gradients in the measured wave heights were observed in the lee of the arrays, resulting in radiation stresses directed alongshore from regions of higher to lower wave energy. This has also been previously shown in numerical models in Refs. [21,40]. Longshore gradients in radiation stresses can also be expected when the wave field direction is oblique to the shoreline, either locally from the diffracted wave field and/or globally from the incident wave field. While the effect of wave direction was not explicitly explored in the experiments reported here [40], shows that radiation stresses induced by wave height gradients in the lee of the WEC array remain significant even under oblique wave conditions.

Two distinct modes of wave height reduction were identified in the lee of the tested WEC arrays (Fig. 7). For the “Breakwater” Configuration in which all WECs were arranged in a shore-parallel line without gaps, wave height reduction was primarily a result of the diffracted wave field. As such, additional radiation stresses were induced in response to the oblique wave fronts associated with the diffracted wave field. In contrast, the resulting wave height reduction from the remaining, WEC arrays was mainly attributed to the radiated wave field arising from WEC-to-WEC interactions. As such, the radiation stresses present in the lee of these other four WEC array configurations were primarily a result of the longshore wave height gradients alone.

The induced radiation stresses were observed to result in the generation of longshore currents. In regions where the local longshore radiation stresses were less evident (e.g., regions of unchanging wave heights), the longshore currents in the wave basin were observed to disperse and shift offshore. This, in turn, resulted in the formation of circulation cells whose size, shape, and direction were observed to depend on wave period, wave height, and the transmitted wave field. As all tests presented in this study were conducted with a shore-normal incident wave field, these observed longshore currents arose from WEC-induced wave height gradients and wave diffraction, not incident wave obliquity.

The wave-induced energy (resulting from nearshore wave height, wave period and nearshore current velocity) determined the movement, accumulation and erosion of sediment that was observed along the shoreline. In regions where the energy exceeded the threshold required to suspend and mobilise sediment, transport occurred in the direction of the current. Where this region of higher energy corresponded to a region where the current dispersed and shifted offshore, sediment was transported offshore, and erosion of the shoreline was observed. Conversely, where energy levels dropped below the sediment transport threshold, sediment deposition occurred, forming a salient and widening of the beach. Importantly, these experiments highlight that wave height shadowing alone is not sufficient to predict the coastal impact of WEC arrays installed near the shore.

As long as an adequate supply of sediment remained in the source regions and following an initial more rapid rate of shoreline adjustment (‘Stage 1’ – refer to Fig. 10) the shoreline recession rates observed in the wave basin for all WEC array configurations were observed to result in a reduced and quasi-steady recession rate. However, in the absence of sediment replenishment, substantial beach erosion is likely to occur.

These results support findings from Ref. [11] which show that both the scattered and radiated wave field contribute to wave height gradients and nearshore circulation patterns. As wave-averaged models –

which only consider the scattered wave field – are the most common numerical approach to modelling coastal protection via WEC arrays, further research is required to assess the sensitivity of sediment transport models to this simplification.

The experimental insights into the wave processes discussed above are expected to be relevant across scales where gravity waves and nearshore hydrodynamic processes dominate and where key non-dimensional parameters and relative geometric proportions are preserved. The experimental design therefore focussed on the relative dimensional proportions of the wave conditions, WEC size and bathymetry, rather than specific scaling of a prototype installation site or WEC design. Under these assumptions, the wave field and associated nearshore hydrodynamic processes may be interpreted using Froude scaling. However, direct extrapolation to prototype-scale shoreline response should be made with caution, as sediment transport, turbulence, viscous effects and device-specific PTO behaviour may introduce additional scale effects. Scale effects also impact the extrapolation of the power output from the OWC devices which is influenced by air compressibility effects [34], and the behaviour of the lightweight sediment used in the experiments which does not directly replicate prototype sediment dynamics and therefore cannot be used to assess volumetric changes to the beach [30]. Additionally, wave basin wall effects may influence circulation currents and reflect obliquely scattered wave. As such, while the wave processes identified are broadly transferable across scales, direct numerical comparisons to the power output or shoreline morphology are best conducted at the experimental scale e.g., Ref. [21].

A primary method of controlling WEC array power absorption is through adjusting resonant properties, array layout, or implementing active control strategies. While these strategies are typically optimised to improve power output or cost, they may also influence the location or volume of sediment deposition. Storm protection strategies also differ greatly between WEC types, ranging from fully passive behaviour e.g., Ref. [41] to highly reflective structures e.g., Ref. [42], meaning coastal protection strategies must consider operational demands. One operational approach could be to increase beach width during ambient wave conditions, improving resilience during extreme events when WEC arrays may not operate. Importantly, optimisation strategies for WEC array design must be site and goal specific and consider the full range of expected wave conditions. As no two sites are identical, no two solutions will likely be identical.

5. Conclusions

This paper presents results from an extensive series of wave basin experiments incorporating a mobile lightweight sediment 'beach' in the presence of WEC arrays. The impacts of different WEC array configurations on nearshore process and shoreline realignment for varying incident wave conditions were observed. This study aimed to explore how well-known coastal engineering concepts interplay with WEC array design principles to influence nearshore process and the resulting shoreline response. By comparing shoreline responses with and without WEC arrays for different wave conditions, distinct shoreline and nearshore responses were observed with the underlying hydrodynamic processes identifiable through the observations and analyses presented.

The experimental observations presented here confirm and emphasise that, while WEC arrays hold promise for dual-purpose power generation and beach erosion mitigation, careful consideration of site-specific sediment dynamics is essential. Other factors include the careful consideration of sediment sources, sinks and pathways, as well as factors influencing the formation and characteristics of nearshore currents circulation cells that are induced by the presence of an WEC array. Beyond the variables explored in this study, other factors such as local bathymetry and the distance of the WEC array to the shore have also been identified as important considerations e.g., Ref. [11].

These experiments also now provide a robust set of observations and results that can serve as a valuable resource for other researchers, for example in testing and evaluating existing and new numerical models that aim to assess WEC array effects on sediment transport and shoreline responses. Comparisons with the results of this study may also assist in identifying the critical processes and parameters that must be accurately simulated to ensure reliable predictions of the wider effects of WECs arrays on their surrounding marine and coastal environments. Once validated, these models could then be applied to more site-specific scenarios, enabling a deeper exploration of WEC array configurations tailored to unique coastal environments and their respective sediment transport regimes.

CRediT authorship contribution statement

Nadav Cohen: Conceptualization, Data curation, Investigation, Methodology, Software, Visualization, Writing – original draft, Writing – review & editing. **Francois Flocard:** Conceptualization, Funding acquisition, Methodology, Project administration, Resources, Supervision, Writing – review & editing. **Lidong Cui:** Conceptualization, Investigation, Methodology, Software, Writing – review & editing. **Nataliia Y. Sergiienko:** Conceptualization, Investigation, Methodology, Software, Writing – review & editing. **Justin S. Leontini:** Conceptualization, Investigation, Methodology, Software, Writing – review & editing. **Ian L. Turner:** Conceptualization, Funding acquisition, Methodology, Project administration, Supervision, Writing – review & editing.

Declaration of competing interest

The authors declare the following financial interests/personal relationships which may be considered as potential competing interests: Nadav Cohen, Francois Flocard, Lidong Cui, Nataliia Y. Sergiienko, Justin S. Leontini, and Ian L. Turner report financial support was provided by Australian Research Council, Mid West Ports Authority and Moyne Shire Council. Nadav Cohen reports financial support was provided by Australian Government Research Training Program Scholarship. If there are other authors, they declare that they have no known competing financial interests or personal relationships that could have appeared to influence the work reported in this paper.

Acknowledgements

This work was funded by the Australian Research Council (ARC), Mid West Ports Authority, and Moyne Shire Council under ARC LP180101109 'Controlling Coastlines While Generating Power'.

NC was also supported by the Australian Government Research Training Program Scholarship at UNSW.

The authors would like to thank Ben Cazzolato and Richard Manasseh for their helpful discussions throughout the experimental campaign.

Further thanks to Dave Clouston, Larry Paice, Mathew Gropp and Caelan Hearne in the construction and running of the experiments.

Data availability

The raw and processed data required to reproduce the above findings are available upon request.

References

[1] C. Ozkan, K. Perez, T. Mayo, The impacts of wave energy conversion on coastal morphodynamics, Sci. Total Environ. 712 (2020), https://doi.org/10.1016/j.scitotenv.2019.136424.

[2] United States Army Corps of Engineers, Coastal Engineering Manual Part VI, Coastal Engineering Manual, U.S. Army Corps of Engineers, Washington, D.C., 2006.

[3] J. Bosboom, M.J.F. Stive, Coastal Dynamics, TU Delft Open, Delft, The Netherlands, 2021.
[4] M. Göteman, M. Giassi, J. Engström, J. Isberg, Advances and challenges in wave energy park optimization—A review, Front. Energy Res. 8 (2020) 26, https://doi.org/10.3389/FENRG.2020.00026, 26.
[5] H. Wolgamot, W. Ebeling, J. Orszaghova, A. Kurniawan, K. McInnes, R. Manasseh, P. Osman, N. Sergiienko, R. Trebilco, P. Marsh, H. Breakey, P. Lyons, B. Jay, T. Denniss, B. Fulton, K. Sprogis, C. Frid, L. Bossi, A. Spencer-Cotton, C. Sampford, J. Melbourne-Thomas, C. Gaudin, Ocean Wave Energy in Australia, Technical Report, Blue Economy, CRC, 2024.
[6] D.L. Millar, H.C.M. Smith, D.E. Reeve, Modelling analysis of the sensitivity of shoreline change to a wave farm, Ocean. Eng. 34 (5) (2007) 884–901, https://doi.org/10.1016/j.oceaneng.2005.12.014.
[7] M. Moradi, N. Chertouk, A. Ilinca, Modelling of a wave energy converter impact on coastal erosion, a case Study for palm Beach-Azur, Algeria, Sustainability 14 (24) (2022), https://doi.org/10.3390/su142416595.
[8] R.J. Bergillos, C. Rodriguez-Delgado, G. Iglesias, Wave farm impacts on coastal flooding under sea-level rise: a case study in southern Spain, Sci. Total Environ. 653 (2019) 1522–1531, https://doi.org/10.1016/j.scitotenv.2018.10.422.
[9] T. Flanagan, M. Wengrove, B. Robertson, Coupled wave energy converter and nearshore wave propagation models for coastal impact assessments, J. Mar. Sci. Eng. 10 (3) (2022), https://doi.org/10.3390/jmse10030370.
[10] D.P. Rijnsdorp, J.E. Hansen, R.J. Lowe, Understanding coastal impacts by nearshore wave farms using a phase-resolving wave model, Renew. Energy 150 (2020) 637–648, https://doi.org/10.1016/j.renene.2019.12.138.
[11] D.R. David, D.P. Rijnsdorp, J.E. Hansen, R.J. Lowe, M.L. Buckley, Predicting coastal impacts by wave farms: a comparison of wave-averaged and wave-resolving models, Renew. Energy 183 (2022) 764–780, https://doi.org/10.1016/j.renene.2021.11.048.
[12] J. Abanades, D. Greaves, G. Iglesias, Coastal defence using wave farms: the role of farm-to-coast distance, Renew. Energy 75 (2015) 572–582, https://doi.org/10.1016/j.renene.2014.10.048.
[13] C. Rodriguez-Delgado, R.J. Bergillos, M. Ortega-Sánchez, G. Iglesias, Wave farm effects on the coast: the alongshore position, Sci. Total Environ. 640–641 (2018) 1176–1186, https://doi.org/10.1016/j.scitotenv.2018.05.281.
[14] C. Rodriguez-Delgado, R.J. Bergillos, G. Iglesias, Dual wave farms and coastline dynamics: the role of inter-device spacing, Sci. Total Environ. 646 (2019) 1241–1252, https://doi.org/10.1016/j.scitotenv.2018.07.110.
[15] J. Abanades, D. Greaves, G. Iglesias, Coastal defence through wave farms, Coast. Eng. 91 (2014) 299–307, https://doi.org/10.1016/j.coastaleng.2014.06.009.
[16] R.J. Bergillos, A. López-Ruiz, E. Medina-López, A. Moñino, M. Ortega-Sánchez, The role of wave energy converter farms on coastal protection in eroding deltas, guadalfeo, southern Spain, J. Clean. Prod. 171 (2018) 356–367, https://doi.org/10.1016/j.jclepro.2017.10.018.
[17] E. Mendoza, R. Silva, B. Zanuttigh, E. Angelelli, T.L. Andersen, L. Martinelli, J. Quvang, H. Nørgaard, P. Ruol, T. Lykke Andersen, L. Martinelli, J.Q. H. Nørgaard, P. Ruol, Beach response to wave energy converter farms acting as coastal defence, Coast. Eng. 87 (2014) 97–111, https://doi.org/10.1016/j.coastaleng.2013.10.018.
[18] B. Battisti, G. Giorgi, G.V. Fernandez, Balancing power production and coastal protection: a bi-objective analysis of Wave Energy Converters, Renew. Energy 220 (2024) 119702, https://doi.org/10.1016/j.renene.2023.119702.
[19] L. Cui, N.Y. Sergiienko, J.S. Leontini, N. Cohen, L.G. Bennetts, B. Cazzolato, I. L. Turner, F. Flocard, A.-R. Westcott, F. Cheng, R. Manasseh, Protecting coastlines by offshore wave farms: on optimising array configurations using a corrected far-field approximation, Renew. Energy 224 (2024) 120109, https://doi.org/10.1016/j.renene.2024.120109.
[20] A. Boodoo, A multi-objective optimization framework for wave farm design: balancing coastal protection and energy output, Renew. Energy Focus 58 (2026) 100831, https://doi.org/10.1016/j.ref.2026.100831.
[21] L. Cui, N.Y. Sergiienko, N. Cohen, J.S. Leontini, B.S. Cazzolato, F. Flocard, R. Manasseh, Coastal response to wave energy converter arrays: a semi-analytical model for control of nearshore currents and beach morphology, Renew. Energy 263 (2026) 125497, https://doi.org/10.1016/j.renene.2026.125497.
[22] V. Stratigaki, P. Troch, T. Stallard, D. Forehand, J.P. Kofoed, M. Folley, M. Benoit, A. Babarit, J. Kirkegaard, Wave basin experiments with large wave energy converter arrays to study interactions between the converters and effects on other users in the sea and the coastal area, Energies 7 (2) (2014) 701–734, https://doi.org/10.3390/en7020701.
[23] L. O'Boyle, B. Elsäßer, T. Whittaker, Experimental measurement of wave field variations around wave energy converter arrays, Sustainability 9 (1) (2017) 1–16, https://doi.org/10.3390/su9010070.
[24] B. Zanuttigh, E. Angelelli, Experimental investigation of floating wave energy converters for coastal protection purpose, Coast. Eng. 80 (2013) 148–159, https://doi.org/10.1016/j.coastaleng.2012.11.007.
[25] S. John Ashlin, S.A. Sannasiraj, V. Sundar, Performance of an array of oscillating water column devices integrated with an offshore detached breakwater, Ocean. Eng. 163 (2018) 518–532, https://doi.org/10.1016/j.oceaneng.2018.05.043.
[26] C. Xu, Study of Wave Interaction with Vertical Piles Integrated with Oscillating Water Columns, University of Hawai'i, 2018. Ph.D. thesis).
[27] O. Lancaster, R. Cossu, A. Wuppukondur, A. Astorga Moar, S. Hunter, T.E. Baldock, Experimental measurements of wave-induced scour around a scaled gravity-based oscillating water column Wave energy converter, Appl. Ocean Res. 126 (2022) 103268, https://doi.org/10.1016/j.apor.2022.103268, 103268.
[28] I.L. Turner, V.M. Leyden, R.J. Cox, L.A. Jackson, J.E. McGrath, A. Jackson, J. E. McGrath, Physical model study of the Gold Coast artificial reef, J. Coast Res. 29 (29) (2001).
[29] O. Kocyigit, B. Lin, R.A. Falconer, Modelling sediment transport using a lightweight bed material, Proc. Inst. Civ. Eng. Marit. Eng. 158 (1) (2005) 3–14, https://doi.org/10.1680/maen.2005.158.1.3.
[30] S.A. Hughes, Physical Models and Laboratory Techniques, World Scientific, 1993.
[31] A.F. Nielsen, I.L. Turner, B.M. Miller, V. Leyden, A.D. Gordon, Experiences with physical scale basin modelling using Mobile sediments. Proceedings of 27th Conference on Coastal Engineering, 2000, pp. 2928–2941. Sydney, Australia.
[32] N. Cohen, F. Flocard, I.L. Turner, N. Sergiienko, B. Cazzolato, Experimental investigation into the air compressibility scaling effect on OWC performance and wave height, in: Proceedings of the 15th European Wave and Tidal Energy Conference, 2023, https://doi.org/10.36688/ewtec-2023-242. Bilbao, Spain.
[33] N. Cohen, Wave Energy Converter Array Impacts on Nearshore Processes and Shoreline Realignment, University of New South Wales, 2025, https://doi.org/10.26190/unsworks/31137. Ph.D. thesis).
[34] A.F.O. Falcão, J.C.C. Henriques, Model-prototype similarity of oscillating-water-column wave energy converters, Int. J. Mar. Energy 6 (2014) 18–34, https://doi.org/10.1016/j.ijome.2014.05.002.
[35] L. Cui, J.S. Leontini, R. Manasseh, Optimising layout of wave energy converter arrays with respect to wave amplitude gradients associated with beach erosion, in: 24th Australasian Fluid Mechanics Conference, 2024. Canberra, Australia.
[36] D.E. Hasselmann, M. Dunckel, J.A. Ewing, Directional wave spectra observed during JONSWAP 1973, J. Phys. Oceanogr. 10 (8) (1980) 1264–1280, https://doi.org/10.1175/1520-0485(1980)010<1264:DWSODJ>2.0.CO;2.
[37] M.D. Harley, M.A. Kinsela, CoastSnap: a global citizen science program to monitor changing coastlines, Cont. Shelf Res. 245 (2022) 104796, https://doi.org/10.1016/j.csr.2022.104796.
[38] S.F. Amy, H.L. Jeffrey, Shoreline change as a proxy for subaerial beach volume change, J. Coast Res. (233) (2007) 740–748, https://doi.org/10.2112/05-0442.1, 2007.
[39] J. Falnes, A. Kurniawan, Ocean Waves and Oscillating Systems: Linear Interactions Including Wave-Energy Extraction, 2 ed., Cambridge University Press, Cambridge, 2020.
[40] X. Cao, J. Shi, J. Zheng, C. Zhang, J. Pan, Offshore wave energy converter array poses threat to coasts causing significant rip currents, Phys. Fluids 37 (8) (2025) 086627, https://doi.org/10.1063/5.0279511.
[41] C.L. Hansen, H. Wolgamot, P.H. Taylor, A. Kurniawan, J. Orszaghova, H. Bredmose, Design waves and extreme responses for an M4 floating, hinged wave energy converter, J. Fluid Struct. 133 (2025) 104253, https://doi.org/10.1016/j.jfluidstructs.2024.104253.
[42] A.A.D. Carrelhas, L.M.C. Gato, J.C.C. Henriques, Peak shaving control in OWC wave energy converters: from concept to implementation in the mutriku wave power plant, Renew. Sustain. Energy Rev. 180 (2023) 113299, https://doi.org/10.1016/j.rser.2023.113299.